Fast Numerical Power Loss Calculation for High-Frequency Litz Wires

Stefan Ehrlich, Hans Rossmanith, Marco Sauer, Christopher Joffe, and Martin März

***Abstract*—This article presents a fast numerical calculation method of realistic power losses for high-frequency litz wires. Explicitly, the imperfect structure of litz wires is considered when calculating losses due to an excitation current (skin losses) and external magnetic fields (proximity losses). Calculations of litz wires with more than 1000 strands were performed on a personal computer and have been validated by measurements up to 10 MHz. In the calculation, the impact of the bundle structure on skin and proximity losses is examined. The method allows to select a suitable litz wire for a specific application or to design a litz wire considering realistic twisting structures.**

***Index Terms*—Bundle level, litz wire, numerical calculation, partial element equivalent circuit (PEEC), power losses, proximity effect, real litz wire behavior, simulation, skin effect.**

I. Introduction

THE shortening of time to market is a permanent demand for product development. Thereby, engineers face increasing requirements for system efficiency and the resource-saving use of materials due to environmental and climate protection. In order to achieve the optimum solution, virtual prototyping and the associated system optimization are inevitable. In power electronic systems, the passives, in particular inductive components, take up a considerable part of the installation space and costs. Increasing the switching frequencies seems promising to reduce the size of passive components. With higher frequencies, frequency-dependent losses, especially winding losses, come into focus for system design and optimization. Their time-efficient and exact prediction is decisive for the aforementioned requirements. Winding losses of round wires or foils are determined with a reasonable calculation effort. By contrast, the loss calculation of litz wires using numerical methods such as finite-element method (FEM) is very time consuming due to their complex bundle structure and twisting.

Beyond numerical calculations, some very fast analytical methods have been presented in the literature. All these methods [1]–[3] are based on a separate calculation of skin, internal proximity, and external proximity losses due to their orthogonality in circular litz wires [4]. Subsequently, all particular loss components are summed up [5], which is an accurate approximation for a large number of strands when a complex stranding structure does not cause dominant losses on bundle level. Therefore, skin and proximity losses are modeled by considering the packing of the strands with a fill factor [2], [3]. For a high number of turns, proximity losses dominate in coil windings and the losses caused by the skin effect may be neglected with the asymptotic approximation in [2], [6]. According to the authors in [2], the ideal number and diameter of strands is determined on the basis of this modeling, even if there is a significant skin effect on bundle level, as these loss mechanisms are independent of each other.

Analytical methods like Ferreira [4] use the Bessel function solution derived for an isolated cylinder to calculate the proximity losses in the individual strands of litz wires as if a set of packed cylinders would behave the same. It has been demonstrated that this approach is incorrect, because the boundary conditions are different. However, for strand diameters, small compared to a skin depth, as is a good choice in litz wire, [4] is an adequate approximation [7]. Homogenization methods of the winding material [8]–[10] were developed to address the aforementioned limitations of [4]. Starting from a unit cell, effective parameters such as conductivity and complex permeability are derived. Homogenization methods are used to accelerate calculation performance of FEM [11] when calculating the field distribution in the winding window, because with effective material parameters, individual strands of a litz wire need not be resolved. For certain conductor geometries, method [12], which is based on the analytical solution of the magnetic vector potential and therefore requires no meshing, offers a faster alternative to FEM. It is more accurate than classical homogenization techniques, because no simplifications of the problem are assumed.

For the selection of a litz wire, manufacturability, costs, as well as availability are major objectives. To seriously consider these objectives, nonideal loss properties and thus the complex twisting structure of a litz wire have to be investigated. None of the described methods is suitable for this purpose. The real

Manuscript received February 24, 2020; revised May 25, 2020; accepted July 3, 2020. Date of publication July 10, 2020; date of current version September 22, 2020. This work was supported by the Federal Ministry of Education and Research of Germany in the framework of InKoLeZ Project No.16EMO0238. Recommended for publication by Associate Editor H. Li. *(Corresponding author: Stefan Ehrlich.)*

Stefan Ehrlich, Marco Sauer, and Christopher Joffe are with the Fraunhofer Institute for Integrated Sytsems and Device Technology IISB, 91058 Erlangen, Germany (e-mail: stefan.ehrlich@iisb.fraunhofer.de; marco.sauer@iisb.fraunhofer.de; christopher.joffe@iisb.fraunhofer.de).

Hans Rossmanith is with the Chair of Electromagnetic Fields, Friedrich-Alexander University Erlangen-Nürnberg, 91054 Erlangen, Germany (e-mail: hans.rossmanith@fau.de).

Martin März is with the Fraunhofer Institute for Integrated Sytsems and Device Technology IISB, 91058 Erlangen, Germany, and also with the Chair of Power Electronics, Friedrich-Alexander University Erlangen-Nürnberg, 91054 Erlangen, Germany (e-mail: martin.maerz@iisb.fraunhofer.de).

Color versions of one or more of the figures in this article are available online at https://ieeexplore.ieee.org.

Digital Object Identifier 10.1109/TPEL.2020.3008564

litz wire behavior is measured and modeled in [1] using the analytical loss formulation of an ideal litz and a round wire. Although nonideal litz wire losses have been measured, those effects are not specified in current data sheets. Further analytical methods are [13], [14], where [13] examines the impact of the pitch length and pitch direction on proximity losses. However, a realistic packing of strands into bundles results in a noncircular shape of the bundles. In this case, the calculation of the bundle or sub-bundle diameters is unclear. This seems to be a methodological shortcoming of [13], as the diameter affects the accuracy of the result. Furthermore, it is mandatory for the method in [13] that bundle level effects are small enough to neglect self-shielding effects.

Numerical methods provide a solution to this problem and with the partial element equivalent circuit (PEEC) method probably the most promising one. It has its origins at IBM [15], [16] and was further developed at the Massachusetts Institute of Technology for the calculation of losses in high-frequency litz wires [17]. The PEEC method is based on approximating the field problem with an electrical equivalent circuit and solving an equation system. Although computing time is reduced with this method in comparison to FEM, the discretization of the investigated structures with cuboids still leads to a large number of elements. Accordingly, loss calculations of litz wires with a high number of strands are not feasible on a personal computer [17], [18]. A major step toward reducing the computing time is the adoption of thin conductors in analogy to the antenna theory [19]. Thereby, strands are considered as single discretization elements [20], [21]. However, this eliminates the ability to model the eddy currents within individual strands, which was included in [17]. Hence, there is a need for separate eddy current models. While in [19] an integral formula of the vector potential of an entire strand is indicated, an explicit analytical derivation of the vector potential for a single numerical element is not shown.

For the analysis of proximity losses in a particular transformer or inductor, all described methods still require the external magnetic field or at least the quadratic mean value of the magnetic field amplitude in the winding window. Only in a few special cases, the magnetic field can be determined analytically. In order to determine the external magnetic field with short computing times, as achieved with a static FEM simulation [18], the following assumptions are made: the eddy currents in the strands do not perturb the external magnetic field, and the impact of unequal current distribution in particular bundles on the magnetic field is small. Based on the magnetic field and the specified litz wire currents, the losses are calculated either analytically [7], [13] or numerically, for example, using the PEEC method [18] (also known as *SlicerPro*).

In this article, we introduce a fast numerical power loss calculation for high-frequency litz wires, in analogy to the PEEC method. From the authors' point of view, the method is most similar to [21], even though the exact derivation of the equation system is not shown there. Thus, this article shows the first analytical formula of the vector potential for each numerical strand element. Based on the complex twisting structure, the equivalent circuit for the numerical calculation of strand currents is derived directly from this vector potential. Combining the numerical calculation method of strand currents and the analytical formulas presented in Section II, realistic power losses of litz wires with more than 1000 strands are calculated on a personal computer. Due to the reduction of the computational time, which is shown in Table III, this method is also regarded as a continuation of Zhang's work [17] to calculate realistic litz wire structures. Just like [17], this numerical approach needs a detailed modeling of the inner litz wire structure. Therefore, we present an approach for an algorithm to calculate twisted litz wire structures. Although modeling the exact packing density at the lowest twisting level of a litz wire still needs mathematical refinements, the shown modeling of the litz wire structure already gives very accurate results compared to measurements. Skin losses as well as proximity losses are validated separately for this numerical calculation model in Sections III and IV. To the authors' knowledge, a separate validation of skin and proximity losses in the numerical model have not yet been investigated to this extent in the literature. When investigating the performance differences between constructions with respect to skin and proximity losses, a precise information about the inner litz wire structure in the simulation is provided, which is a significant contribution compared to [21]. External fields in the winding window and near air gaps are computed with FEM as shown in [18].

II. Theory of the Fast Numerical Calculation Method

In the following section, a method (SEEC: strand element equivalent circuit) for the fast calculation of losses in high-frequency litz wires analogous to the PEEC method is introduced. It most closely resembles the method according to [21], which is based on the numerical elements of [19]. Starting from the discrete modeling of the litz wire structure, an equation system for the calculation of the strand currents is derived. In the equation system, both the internal and external magnetic fields are considered.

A. Magnetic Vector Potential of a Strand Element

Litz wires are composed of twisted bundles, which in turn consist of twisted bundles in a recursive manner or single strands, as Fig. 1(a) shows for a $(7 \times 7)_{49}$ litz wire. Due to electromagnetic induction, the currents in the strands of a litz wire affect each other. To take induction effects into account when determining strand currents, the electromagnetic vector potential is used. Whereas in round conductors, the current direction corresponds to the conductor direction, the current conducting twisted strands change their direction along the axis of the of a litz wire [cf. Fig. 1(a)]. Regardless of this, only the vector potential component parallel to the axis direction $\vec{\mathbf{e}}_1$ of a litz wire is relevant, the current in a strand section is assumed to be $\vec{\mathbf{e}}_1$ – paralleled. All strand elements contribute only to this vector potential component, so that a magnetic flux density component parallel to $\vec{\mathbf{e}}_1$ cannot be derived. This simplification has no major impact on the loss calculation in typical windings, because components of the magnetic vector potential orthogonal to the strands will not cause equalizing currents through the

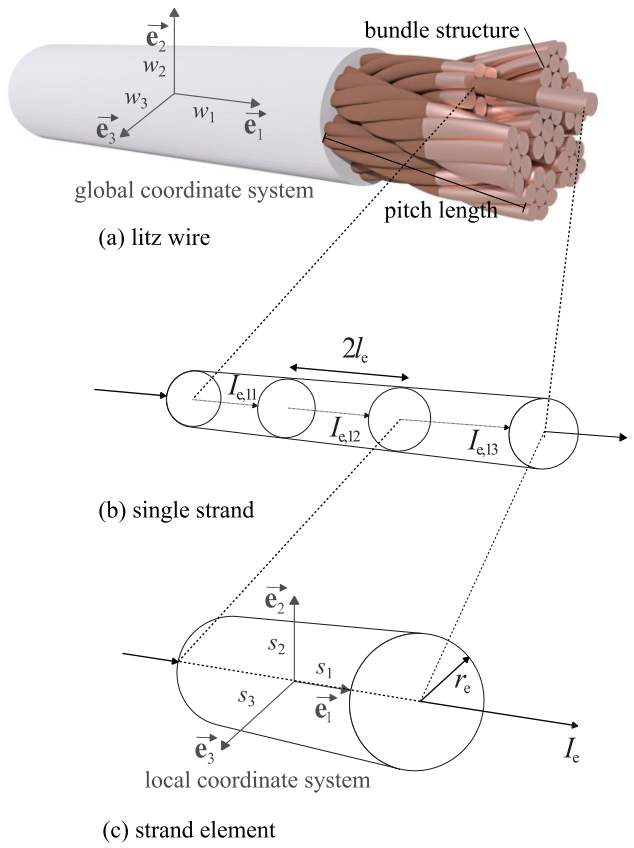

Fig. 1. Figure shows (a) structure of a $(7 \times 7)_{49}$ litz wire with twisted bundles and single strands. The first number inside the brackets indicates the top bundle level with seven bundles and the second number indicates the strand level with seven strands. The subscript number (here 49) describes the total number of strands in the litz wire. To model the electrical behavior of a single strand (b) in the fast numerical calculation, many strand elements are connected in series (c). All strand elements have a radius of r_e and a length of $2l_\mathrm{e}$.

individual strands. However, eddy currents within the strands can be calculated analytically in case of a significant influence.

For the investigation of entire windings of inductive components, where the sections [cf. Fig. 1] have different orientations in space, it is assumed that the litz wire winding is $\vec{\mathbf{e}}_1$ directed. The vector potential on a section of the litz wire is defined as follows:

$$\vec{\mathbf{A}}_\mathrm{litz}\left(\vec{\mathbf{r}}_\mathrm{litz}\right) = A\left(w_1, w_2, w_3\right)\vec{\mathbf{e}}_1$$
$$\text{where } \vec{\mathbf{r}}_\mathrm{litz} = w_1\vec{\mathbf{e}}_1 + w_2\vec{\mathbf{e}}_2 + w_3\vec{\mathbf{e}}_3\ . \tag{1}$$

For the numerical calculation of strand currents, the complex litz wire structure, which is formed by a high number of radially and azimuthally permuted insulated strands [21], is modeled with strand elements in form of small cylinders with the radius r_e and the length $2l_\mathrm{e}$, as shown in Fig. 1. To minimize losses in litz wire applications, the strand radius r_e is chosen to be small compared to the skin depth of the operating frequency range of a litz wire. If eddy currents are induced within the strands by an external magnetic field at higher frequencies, a magnetic field similar to that of a line dipole is generated and superimposed on the exciting field. These dipole fields mainly contribute to the external field of adjacent strands and decrease with the inverse square of the distance. However, for strand diameters small compared to a skin depth, as is a good choice in litz wire, it is acceptable to neglect these effects. The current I_e through a strand element in $\vec{\mathbf{e}}_1$-direction is homogeneous for lower frequencies. Eddy currents within the strands at higher frequencies will be dealt separately in this article.

If a local Cartesian coordinate system with the coordinates $s_1,\ s_2,\ s_3$ [cf. Fig. 1(c)] is placed in the center of a strand element, the strand element with the current I_e has the same vector potential $\vec{\mathbf{A}}_{\mathrm{e},\,\mathrm{o}}$ outside the element as a line current element placed in its center. Using the Biot–Savart formula for the magnetic vector potential of a line current element, the following magnetic vector potential results, where μ_0 is the vacuum permeability, I_e is the current through the strand element, and ρ_e is the distance from the center of a strand element:

$$\vec{\mathbf{A}}_{\mathrm{e},\,\mathrm{o}} = \frac{\mu_0 I_\mathrm{e}}{4\pi}\int_{-l_\mathrm{e}}^{l_\mathrm{e}} \frac{\mathrm{d}s}{\sqrt{\rho_\mathrm{e}^2 + (s_1 - s)^2}}\vec{\mathbf{e}}_1$$
$$= \frac{\mu_0 I_\mathrm{e}}{4\pi}\left[\ln\left(\frac{\sqrt{\rho_\mathrm{e}^2 + (s_1 - l_\mathrm{e})^2} - (s_1 - l_\mathrm{e})}{\sqrt{\rho_\mathrm{e}^2 + (s_1 + l_\mathrm{e})^2} - (s_1 + l_\mathrm{e})}\right)\right]\vec{\mathbf{e}}_1,$$
$$\rho_\mathrm{e} = \sqrt{s_2^2 + s_3^2}\ . \tag{2}$$

Within the cylindrical strand elements, the magnetic vector potential $\vec{\mathbf{A}}_{\mathrm{e,i}}$ is derived from an integration over a homogeneous spatial current density of cylinder hulls with an infinitesimal length $2l_\mathrm{e}$ and a radius ρ_e.

$$\vec{\mathbf{A}}_{\mathrm{e,i}} = \frac{\mu_0 I_\mathrm{e}}{4\pi}\left[\frac{2\pi}{\pi r_\mathrm{e}^2}\int_{\rho_\mathrm{e}}^{r_\mathrm{e}} \ln\left(\frac{\sqrt{r^2 + (s_1 - l_\mathrm{e})^2} - (s_1 - l_\mathrm{e})}{\sqrt{r^2 + (s_1 + l_\mathrm{e})^2} - (s_1 + l_\mathrm{e})}\right) r\mathrm{d}r + \frac{\pi\,\rho_\mathrm{e}^2}{\pi r_\mathrm{e}^2}\ln\left(\frac{\sqrt{{\rho_\mathrm{e}}^2 + (s_1 - l_\mathrm{e})^2} - (s_1 - l_\mathrm{e})}{\sqrt{{\rho_\mathrm{e}}^2 + (s_1 + l_\mathrm{e})^2} - (s_1 + l_\mathrm{e})}\right)\right]\vec{\mathbf{e}}_1,$$
$$\rho_\mathrm{e} = \sqrt{s_2^2 + s_3^2}. \tag{3}$$

The integral is evaluated to simplify the numerical calculation of the vector potential of an element.

$$\vec{\mathbf{A}}_{\mathrm{e,i}} = \frac{\mu_0 I_\mathrm{e}}{4\pi}\left[\begin{array}{c} \ln\left(\frac{\sqrt{r_\mathrm{e}^2 + (s_1 - l_\mathrm{e})^2} - (s_1 - l_\mathrm{e})}{\sqrt{r_\mathrm{e}^2 + (s_1 + l_\mathrm{e})^2} - (s_1 + l_\mathrm{e})}\right) \\ + \frac{s_1 - l_\mathrm{e}}{r_\mathrm{e}^2}\left(\sqrt{\rho_\mathrm{e}^2 + (s_1 - l_\mathrm{e})^2} - \sqrt{r_\mathrm{e}^2 + (s_1 - l_\mathrm{e})^2}\right) \\ - \frac{s_1 + l_\mathrm{e}}{r_\mathrm{e}^2}\left(\sqrt{\rho_\mathrm{e}^2 + (s_1 + l_\mathrm{e})^2} - \sqrt{r_\mathrm{e}^2 + (s_1 + l_\mathrm{e})^2}\right) \end{array}\right]\vec{\mathbf{e}}_1 \tag{4}$$

Equations (2) and (4) provide the contribution of a single strand element to the vector potential of a closed current loop consisting of several such elements. As already indicated in

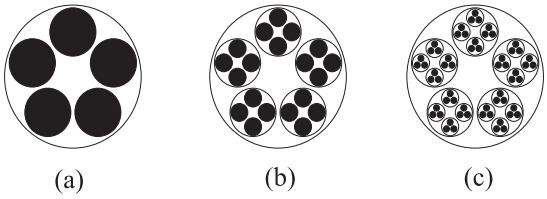

Fig. 2. Initial position of all strands in a litz wire cross-section: Litz wires are composed of several twisted bundles in a recursive manner or of single strands. $(5 \times 4 \times 3)_{60}$ litz wire, which is composed of (a) five twisted bundles at top bundle level, (b) four twisted bundles at a middle bundle level, and (c) three twisted strands at the lowest bundle level (strand level).

Fig. 1(b), the strand currents at the interfaces of the elements within a strand are continuous $I_{\mathrm{e},11} = I_{\mathrm{e},12} = I_{\mathrm{e},13}$.

B. Numerical Stranding of Litz Wires

For the presented numerical calculation of the losses in high-frequency litz wires, the complex structure of a litz wire is modeled discretely. Therefore, a $\vec{\mathbf{e}}_1$-directed litz wire is subdivided into sections with the infinitesimal length $2l_{\mathrm{e}}$ of a strand element [cf. Fig. 1(b) and (c)]. In a section, the magnetic vector potential is evaluated only in the center of a particular strand element, where $s_1 = 0$ is valid in the local coordinate system. Thus, the strand positions are also determined in the center of a strand element on a cross-sectional area perpendicular to the $\vec{\mathbf{e}}_1$ direction.

The stranding procedure for each section of the litz wire is as follows. First, an initial position of all strands in the litz wire cross-section is determined. Thereby, sub-bundle positions are defined by their center coordinates relative to the corresponding bundle center. The sub-bundles are initially placed on a circle around the bundle center, which is applied recursively down to the lowest bundle level (cf. Fig. 2). Once all bundle positions have been determined, an optimization procedure analogous to the placement of components on a printed circuit board begins. Optimized bundle positions are obtained by minimizing an objective function with penalties if partial sub-bundles overlap or exceed the specified cross-section of the litz wire as well as penalties for a large distance of the sub-bundles from their starting positon. Now all bundle positions are fixed. For litz wires with a large number of strands, strand positions will not be part of the optimization, but are placed on a regular lattice within a circular cross-section of the lowest level bundle. The next section along the $\vec{\mathbf{e}}_1$-direction of the litz wire uses starting positions for each sub-bundle of the recursive twisting steps, which are rotated by a certain angle around the bundle center. The strand positions are likewise rotated and the bundle position optimization procedure starts again. The individual strands of successive sections are assumed to be electrically connected.

As an example, an arbitrary cross-section of a litz wire with a $(7 \times 4 \times 35.7)_{1000}$ twisting structure is considered. The decimal number with one digit after the decimal point (here 35.7) represents the average number of strands per sub-bundle. Comparing with the cross-section view of a cut litz wire under the microscope [cf. Fig. 3(b)], it can be seen that in the model the strands are more densely packed into idealized round bundles

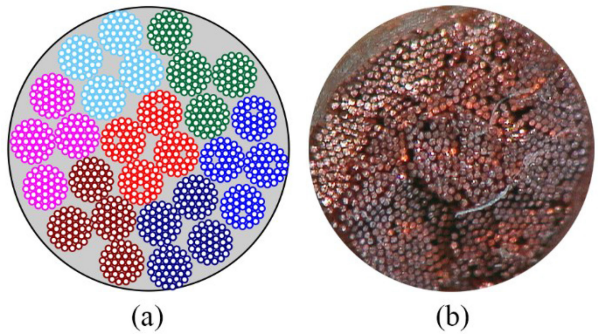

Fig. 3. Individual strand positions in the cross-section of a $(7 \times 4 \times 35.7)_{1000} \times 0.071$ mm (strand diameter) litz wire are shown as they are positioned (a) in the model and (b) for a real litz wire. The twisted sub-bundles of the middle bundle level have the same color in (a). The contours of the bundles are visible in the real litz wire, cf. (b). One bundle of the top bundle level is located in the center of the litz wire.

within the strand level, but have more space between the partial sub-bundles, cf. Fig. 3(a). This approximation may affect the accuracy of the method for large diameters of bundles on strand level.

Litz wires with a high number of strands have several twisting levels (e.g., the litz wire in Fig. 2 with three twisting levels) for two main reasons. On the one hand, the number of strands, which a twisting machine can handle, is limited. On the other hand, if more than five bundles or strands are twisted, there is a group of sub-bundles or strands that stay in the center of a bundle, hence other groups never appear in the center along the entire length of the litz wire (cf. Fig. 3). Such bundles are not permuted radially, resulting in a dramatically increase of skin losses [21]. To model this litz wire structure, it is not feasible to arrange all sub-bundles or strands on a circle at the same distance from the bundle center, as in Fig. 2(a). Instead, these types of sub-bundles are arranged on several concentric circles around the bundle center before the optimization procedure is started. By the optimization, the bundles are placed in the cross-section of a litz wire according to the penalties mentioned above, but they remain close to their starting positions. Thereby, some bundles are closer to the center of the corresponding bundle than others.

Only one litz wire of a particular length, the so-called unit cell, of the entire litz winding is discretely built-up for the numerical calculation. Ideally, the length of this unit cell is chosen as the least common multiple of the pitch lengths of all recursively twisted bundles. To avoid extremely long unit cells, a small deviation from the real pitch length in the model is allowed, in order to minimize the length of the unit cell (cf. Table II). Even an accepted deviation of 5% leads to short unit cells, which is sufficient for the simulation. Note that a unit cell always represents only one possible variant of a given litz wire and it cannot be guaranteed that bundle positions of this variant correspond to those of a real litz wire. Hence, it is valuable to model unit cells with various degrees of freedom. This enables to differentiate which results apply only to the positions of the chosen unit cell and which apply for a real litz wire. Approximately 25 sections within this unit cell provide accurate calculation results. Before calculating losses, the bundle structure has to be created just

TABLE I
CPU TIME ON A PERSONAL COMPUTER (CPU-TYPE: INTEL CORE I7-3632QM; NUMBER OF CORES: 4; RAM MEMORY: 7.8 GB) TO SET UP A UNIT CELL WITH 25 SECTIONS FOR SEVERAL LITZ WIRES

bundle structure	number of strands	CPU time
7 x 35 (*lw 6*, TABLE II)	245	15 sec
7 x 4 x 35.7 (*lw 11*, TABLE II)	1000	60 sec

The stranding procedure is implemented in the programming language MATLAB.

once for a new litz wire. According to Table I, the calculation time of a unit cell is about 1 min for a litz wire with 1000 strands.

Again, it should be emphasized that all strand elements and their currents are assumed to be $\vec{\mathbf{e}}_1$ -directed, parallel to the litz wire direction. Only this $\vec{\mathbf{e}}_1$ -component of the vector potential is evaluated. In summary, the modeling considers the most important structural properties of a litz wire, such as multiple bundle levels, pitch lengths, as well as pitch directions. Bundle configurations with center bundles (cf. Fig. 3), with a noncircular shape and "hollow" litz wire structures in which strands are wound on the outer diameter of a dielectric core (cf. [22]) are also viable with the presented modeling approach. Nevertheless, mathematical refinements are necessary, in particular to accelerate the stranding procedure, if the exact packing density at strand level of a litz wire has to be modeled.

C. Calculation of Strand Currents

For the calculation of winding losses, it is sufficient to restrict the investigations to sinusoidal currents and voltages with different frequencies, due to the linearity of the problem. Using the Fourier expansion, arbitrary periodic waveforms are represented in the complex notation. To connect a litz wire with other electronic components, all strands are electrically connected at their ends, e.g., by solder joints. As all strands are connected in parallel and all strand currents interact with each other by electromagnetic induction, equalizing currents are generated between the single strands. A correlation of the induced voltage $\underline{v}_n$ and the strand currents $\underline{i}_n$ is established by integrating the magnetic vector potential $\underline{A}_n$ along a single strand *n* with a path element $\mathrm{d}w_1$. For the numerical calculation, each integral is a summation of the magnetic vector potentials along the axis of the litz wire with K sections of the length l_{nk} [cf. Fig. 1(a)]

$$\underline{v}_n = j\omega \int \underline{A}_n \, \mathrm{d}w_1 = j\omega \sum_{k=1}^{\mathrm{K}} l_{nk} \underline{A}_{nk} \tag{5}$$

where ω is the angular frequency. The total magnetic vector potential $\underline{A}_{nk}$ at strand *n* on strand element *k* is a superposition of the external vector potential $\underline{A}_{nk,\mathrm{ex}}$ due to an external magnetic field and the sum of all outer vector potentials $\underline{A}_{nk,\mathrm{o}}$, cf. (2) from the strand elements in the litz wire including its own inner vector potential $\underline{A}_{nk,\mathrm{i}}$, cf. (4). Excluding some specific situations,

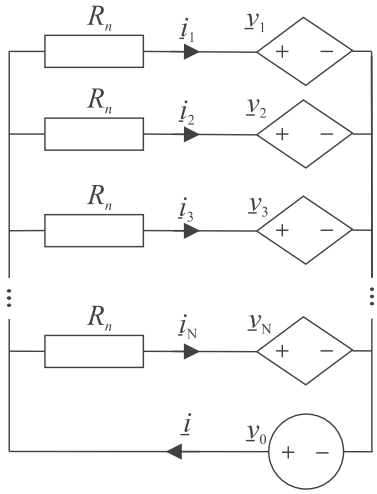

Fig. 4. Equivalent circuit diagram of a litz wire with *N* strands.

especially with air gaps, the external magnetic field may be assumed as homogeneous over the cross-section of a litz wire. Evaluating the field in the center of the litz wire cross-section is reasonable. A magnetic field component parallel to $\vec{\mathbf{e}}_1$ is neglected here, as it has no influence on the equalizing strand currents [13]. So, the external magnetic vector $\vec{\mathbf{A}}_{\mathrm{ex}}$ potential is determined directly from the external magnetic field $\vec{\mathbf{H}}_{\mathrm{ex}}$

$$\vec{\mathbf{A}}_{\mathrm{ex}} = \underline{A}_{\,nk,\mathrm{ex}}\,(w_1, w_2, w_3)\,\vec{\mathbf{e}}_1 = \mu_0 \left(\underline{H}_{\,\mathrm{e}_2} w_3 - \underline{H}_{\,\mathrm{e}_3} w_2\right) \vec{\mathbf{e}}_1$$
$$\text{where } \vec{\mathbf{H}}_{\mathrm{ex}} = \underline{H}_{\,\mathrm{e}_2}\,(w_1)\,\vec{\mathbf{e}}_2 + \underline{H}_{\,\mathrm{e}_3}\,(w_1)\,\vec{\mathbf{e}}_3\,. \tag{6}$$

For the calculation of $\underline{A}_{nk}$ in the center of the particular strand element according to (2), (4), the following applies:

$$\vec{\mathbf{A}}_{\mathrm{e,o}} = \underline{A}_{nk,\mathrm{o}}\,(s_1, \rho_{nk})\,\vec{\mathbf{e}}_1 \quad \text{and} \quad \vec{\mathbf{A}}_{\mathrm{e,i}} = \underline{A}_{nk,\mathrm{i}}\,(s_1, 0)\,\vec{\mathbf{e}}_1. \tag{7}$$

With these $\vec{\mathbf{e}}_1$ -components of the magnetic vector potential, (5) is written as:

$$\underline{v}_{\,n} = j\omega \sum_{k=1}^{\mathrm{K}} \left[l_{nk}\, \underline{A}_{nk,\mathrm{ex}} + l_{nk}\, \underline{A}_{nk,\mathrm{i}} + \sum_{\eta=1,\eta\neq nk}^{\mathrm{NK}} l_{nk\eta}\, \underline{A}_{nk\eta,\mathrm{o}} \right]$$
$$= \underline{v}_{\,n,\mathrm{ex}} + \underline{v}_{\,n,\mathrm{int}}. \tag{8}$$

The voltages $\underline{v}_{\,n}$ in the single strands are induced by external magnetic fields $(\underline{v}_{\,n,\mathrm{ex}})$ and internal strand currents $(\underline{v}_{\,n,\mathrm{int}})$. The electrical behavior of a litz wire is described by the equivalent circuit diagram in Fig. 4. In a litz wire, the dc resistance of all *N* strands may not be identical in general. Due to the first construction step, where often more than 20 strands are twisted together, some strands may have a shorter path in the middle of the bundle than in outer positions of the bundle. Assuming the same resistance $R_n = NR_{\mathrm{dc}}$ for all strands, where R_{dc} is the dc resistance of the litz wire, however, has only a minor effect on litz wire losses [21]. If a differentiation of the resistances would be necessary, the individual dc resistors might be obtained from

the positioning of the strands in a unit cell. The ac resistance of the strands is of secondary relevance, because at lower frequencies the dc resistance and at higher frequencies the inner proximity losses, due to the magnetic field of all strands in the litz wire, are dominant over the strand skin losses.

The voltage $\underline{v}_n$ induced in a single strand *n* is represented by a current-controlled voltage source. At both nodes of the circuit, all strand currents $\underline{i}_n$ are added up to the current of the litz wire $\underline{i}$. An additional voltage source $\underline{v}_0$ in a fictive return path allows adjusting current $\underline{i}$ to the given value. According to Kirchhoff's current law, the following applies:

$$\underline{i} = \sum_{n=1}^{N} \underline{i}_n = \sum_{n=1}^{N} \frac{\underline{v}_0 - \underline{v}_n}{R_n} \,. \tag{9}$$

Assuming identical dc resistances $R_n = NR_{\mathrm{dc}}$ for all strands, a mathematical transformation of (9) results in an expression for the fictive voltage $\underline{v}_0$

$$\underline{v}_0 = R_{\mathrm{dc}}\,\underline{i} + \underline{v} \quad \text{where} \quad \underline{v} = \frac{1}{N}\sum_{n=1}^{N} \underline{v}_n \,. \tag{10}$$

By applying Kirchhoff's voltage law for the equivalent circuit in Fig. 4 and using (10) and (11) is derived in matrix notation, where $\underline{\mathbf{I}}$ is the vector of the strand currents, $\underline{\mathbf{V}}$ is the vector of induced voltages in the strands, and $\mathbf{1}$ is a vector with *N* identical components 1

$$\underline{\mathbf{I}} = \frac{1}{R_n}\ (\mathbf{1}\underline{v}_0 - \underline{\mathbf{V}}) = \frac{1}{NR_{\mathrm{dc}}}\ (R_{\mathrm{dc}}\,\mathbf{1}\,\underline{i} - \underline{\mathbf{V}} + \mathbf{1}\,\underline{v})$$

$$\text{where}\ \ \underline{\mathbf{V}} = [\underline{v}_1, \underline{v}_2, \ldots, \underline{v}_n, \ldots, \underline{v}_{\mathrm{N}}]^{\mathrm{T}}$$

$$\underline{\mathbf{I}} = [\underline{i}_1, \underline{i}_2, \ldots, \underline{i}_n, \ldots, \underline{i}_{\mathrm{N}}]^{\mathrm{T}}$$

$$\mathbf{1} = [1, 1, \ldots, 1, \ldots, 1]^{\mathrm{T}}. \tag{11}$$

In (11), the total current $\underline{i}$, the dc resistance R_{dc}, as well as the number of strands *N* are known parameters. The voltages $\underline{v}_n$ depend on the magnetic vector potential, which again depends on the strand current $\underline{i}_n$ [cf. (2), (4), and (8)]. If the external magnetic field is also known, all quantities with the exception of the strand currents are determined. To calculate the strand currents, the linear equation system

$$\underline{\mathbf{M}} \cdot \underline{\mathbf{I}} = \underline{\mathbf{b}} \quad \text{and} \quad \underline{\mathbf{I}} = [\underline{i}_1, \underline{i}_2, \ldots, \underline{i}_m, \ldots \underline{i}_{\mathrm{N}}]^{\mathrm{T}}$$

$$\underline{\mathbf{b}} = [\underline{b}_1, \underline{b}_2, \ldots, \underline{b}_n, \ldots \underline{b}_{\mathrm{N}}]^{\mathrm{T}} \tag{12}$$

is solved with the Software MATLAB. Thereby all known quantities are summarized in the vector $\underline{\mathbf{b}}$

$$\underline{\mathbf{b}} = R_{\mathrm{dc}}\ \mathbf{1}\,\underline{i} - \underline{\mathbf{V}}_{\mathrm{ex}} + \mathbf{1}\,\underline{v}_{\mathrm{ex}}$$

$$\text{where}\ \ \underline{v}_{\mathrm{ex}} = \frac{1}{N}\sum_{n=1}^{N} \underline{v}_{n,\mathrm{ex}}$$

$$\underline{\mathbf{V}}_{\mathrm{ex}} = [\underline{v}_{1,\mathrm{ex}}, \underline{v}_{2,\mathrm{ex}}, \ldots, \underline{v}_{n,ex}, \ldots, \underline{v}_{\mathrm{N,ex}}]^{\mathrm{T}}. \tag{13}$$

Any terms linked with the strand currents are found in the quadratic matrix $\underline{\mathbf{M}}$

$$\underline{\mathbf{M}} = \left[\begin{pmatrix} R_n & \cdots & 0 \\ \vdots & \ddots & \vdots \\ 0 & \cdots & R_n \end{pmatrix}^{\mathrm{NxN}} + \begin{pmatrix} \underline{\zeta}_{11} & \cdots & \underline{\zeta}_{1m} & \cdots & \underline{\zeta}_{1\mathrm{N}} \\ \vdots & \ddots & \vdots & \ddots & \vdots \\ \underline{\zeta}_{n1} & \cdots & \underline{\zeta}_{nm} & \cdots & \underline{\zeta}_{n\mathrm{N}} \\ \vdots & \ddots & \vdots & \ddots & \vdots \\ \underline{\zeta}_{\mathrm{N}1} & \cdots & \underline{\zeta}_{\mathrm{N}m} & \cdots & \underline{\zeta}_{\mathrm{NN}} \end{pmatrix}^{\mathrm{NxN}} \right] \tag{14}$$

where along row *n*, the influence of the strand currents $[\underline{i}_1, \underline{i}_2, \ldots, \underline{i}_m, \ldots \underline{i}_{\mathrm{N}}]$ on the induced voltage of strand *n* is evaluated. According to (14), all induced voltages $\underline{v}_{nm,\mathrm{int}}$ of the K sections, which are caused by the strand current *m*, forming the strand *n* are summarized in $\underline{\zeta}_{nm}$

$$\underline{\zeta}_{nm} = \frac{\underline{v}_{nm,\mathrm{int}}}{\underline{i}_m}. \tag{15}$$

For all calculations of strand currents, the strand elements have an equal length $l_{nk} = 2l_{\mathrm{e}}$ and an equal radius of a litz wire strand $r_{\mathrm{e}} = r_{\mathrm{s}}$, cf. Fig. 1. In the following, strand currents are assumed to be known.

D. Loss Calculation in Litz Wires

Using the frequency-dependent ac resistance of a single strand $R_{\mathrm{strand,ac}}$ and the strand currents from (12), the losses in the litz wire strands P_{curr} are calculated

$$P_{\mathrm{curr}} = \sum_m |\underline{i}_m|^2 R_{\mathrm{strand,ac}} \quad \text{where} \quad R_{\mathrm{strand,ac}} = NR_{\mathrm{dc}}\,D_{\mathrm{s}}$$

$$D_{\mathrm{s}} = \frac{1}{2}\mathrm{Re}\left\{\frac{\alpha r_{\mathrm{s}} \mathrm{I}_0(\alpha r_{\mathrm{s}})}{\mathrm{I}_1(\alpha r_{\mathrm{s}})}\right\}\,,\ \ \alpha = (1+j)\sqrt{\pi f \kappa \mu_0}\,. \tag{16}$$

The single strand skin factor D_{s} describes the increase of the resistance of a single strand due to the skin effect determined with Bessel functions I_0, I_1 [1], *f* is the frequency, κ is the conductivity, and *N* is the number of the litz wire strands. Eddy currents generated within the individual strands due to the proximity effect are thus ignored. Internal and external proximity losses within the strands must therefore be calculated separately and added up. The proximity losses within a strand depend on the amplitude of the total incident magnetic field $\hat{H}$, including the internal and external field [13]. With small diameters, $\hat{H}$ is unlikely to change significantly over the cross-section of the strands and the Bessel function solution [4], [7] derived for homogeneous magnetic fields, is used to calculate the proximity losses $P_{\mathrm{H-field,e}}$ in a given strand element

$$P_{\mathrm{H-field,e}} = \frac{1}{\kappa} 2l_{\mathrm{e}} D_{\mathrm{p}} \hat{H}^2$$

$$\text{where} \quad D_{\mathrm{p}} = 2\pi \mathrm{Re}\left\{\frac{\alpha r_{\mathrm{s}} \mathrm{I}_1(\alpha r_{\mathrm{s}})}{\mathrm{I}_0(\alpha r_{\mathrm{s}})}\right\}. \tag{17}$$

Herein, D_{p} is the proximity factor of a single strand [1]. Not considering self-shielding effects due to eddy currents within the

strands is reasonable, because litz wire using strands sufficiently small compared to skin depth nearly eliminates the self-shielding effects. The internal field at a given strand element is the superposition of all contributions $\vec{\mathbf{H}}_{\mathrm{eo}}$ generated by the strand elements of a unit cell except the strand elements of the considered strand. The field $\vec{\mathbf{H}}_{\mathrm{eo}}$ results from the curl operation of the magnetic vector potential (2):

$$\vec{\mathbf{H}}_{\mathrm{eo}} = \frac{1}{\mu_0}\left(\nabla \times \vec{\mathbf{A}}_{\mathrm{e,\,o}}\left(s_1, \rho_{\mathrm{e}}\right)\right) = -\frac{1}{\mu_0}\frac{\partial}{\partial \rho_{\mathrm{e}}}\left(\vec{\mathbf{A}}_{\mathrm{e,\,o}}\left(s_1, \rho_{\mathrm{e}}\right) \cdot \vec{\mathbf{e}}_1\right)\vec{\mathbf{e}}_{\varphi}$$

$$\text{where } \rho_{\mathrm{e}} = \sqrt{s_2^2 + s_3^2} \text{ and } \vec{\mathbf{e}}_{\varphi} = -\frac{s_3}{\rho_{\mathrm{e}}}\vec{\mathbf{e}}_2 + \frac{s_2}{\rho_{\mathrm{e}}}\vec{\mathbf{e}}_3. \tag{18}$$

The field components $\vec{\mathbf{H}}_{\mathrm{eo,e_2}}$ and $\vec{\mathbf{H}}_{\mathrm{eo,e_3}}$ generated by a single strand element result from (18) and (2) as follows:

$$\vec{\mathbf{H}}_{\mathrm{eo,e_2}} = \frac{I_{\mathrm{e}}}{4\pi}\left(\frac{s_1 - l_{\mathrm{e}}}{\sqrt{\left(s_1 - l_{\mathrm{e}}\right)^2 + \rho_{\mathrm{e}}^2}} - \frac{s_1 + l_{\mathrm{e}}}{\sqrt{\left(s_1 + l_{\mathrm{e}}\right)^2 + \rho_{\mathrm{e}}^2}}\right)\frac{s_3}{\rho_{\mathrm{e}}^2}\vec{\mathbf{e}}_2$$

$$\vec{\mathbf{H}}_{\mathrm{eo,e_3}} = -\frac{I_{\mathrm{e}}}{4\pi}\left(\frac{s_1 - l_{\mathrm{e}}}{\sqrt{\left(s_1 - l_{\mathrm{e}}\right)^2 + \rho_{\mathrm{e}}^2}} - \frac{s_1 + l_{\mathrm{e}}}{\sqrt{\left(s_1 + l_{\mathrm{e}}\right)^2 + \rho_{\mathrm{e}}^2}}\right)\frac{s_2}{\rho_{\mathrm{e}}^2}\vec{\mathbf{e}}_3\,. \tag{19}$$

For the calculation of the internal field at the individual strand elements the strand currents $\underline{\mathbf{I}}$ are used. As mentioned before, the external magnetic field over the cross-section is considered to be only a function of w_1 in the direction of the litz wire. The superposition of all magnetic fields results in $\hat{H}$ and the proximity losses of a given strand element are determined using (17). Analogously, the losses of all remaining strand elements are calculated and finally summed up to total losses $P_{\mathrm{H-field}}$. Note that a separate calculation of the losses in (16) and (17) is valid for all types of litz wire consisting of strands with a round cross-section [4], [7]. The assumption that magnetic fields of eddy currents within the strands compensate each other at neighboring strands is no longer valid for highly oblong cross-sections of the litz wire and for small numbers of strands [7]. It is expected that the method is very accurate for typical litz wires with a round or rectangular cross-section.

In the case of litz wires with a round cross-section, the proximity losses $P_{\mathrm{H-field}}$ due to the internal and external magnetic field may also be determined separately [7]. Those losses only depend on the quadratic mean value of the field amplitude $\overline{\hat{H}^2}$. As the internal magnetic field of a straight round wire section with a homogeneous current density in the center of the cross-section is zero, the external field corresponds to the total field in the wire center. Thus, after a static FEM simulation with homogeneous current densities as in [18], the external magnetic field on a center path of the wire is known. So we recommend to calculate the quadratic mean value $\overline{\hat{H}^2}_{\mathrm{ex}}$ along the litz wire path. The quadratic mean value for the internal field $\overline{\hat{H}^2}_{\mathrm{in}}$ should be computed over all strand elements of a unit cell to ensure that the entire twisting structure of the litz wire is considered.

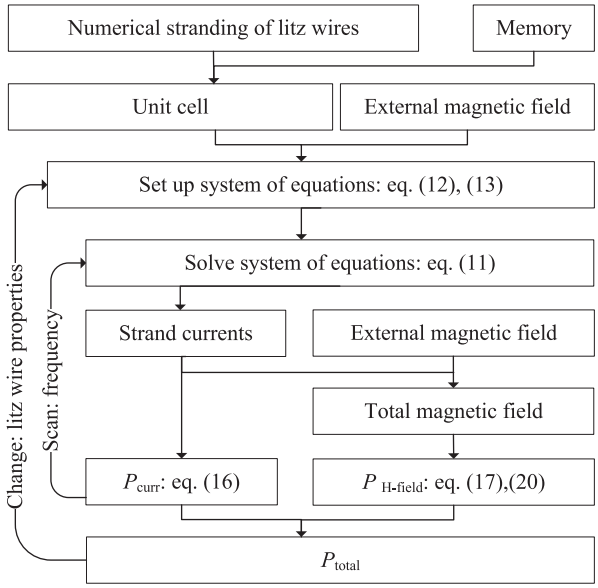

Fig. 5. Schematic work flow of the SEEC method.

$$P_{\mathrm{H-field}} = \frac{1}{\kappa} l_{\mathrm{litz}} N D_{\mathrm{p}}\left(\overline{\hat{H}^2}_{\mathrm{int}} + \overline{\hat{H}^2}_{\mathrm{ex}}\right)$$

$$\text{where} \quad D_{\mathrm{p}} = 2\pi \mathrm{Re}\left\{\frac{\alpha r_{\mathrm{s}} \mathrm{I}_1\left(\alpha r_{\mathrm{s}}\right)}{\mathrm{I}_0\left(\alpha r_{\mathrm{s}}\right)}\right\}. \tag{20}$$

In this equation, l_{litz} is the length of the litz wire. Total losses P_{tot} are calculated as follows:

$$P_{\mathrm{tot}} = P_{\mathrm{curr}} + P_{\mathrm{H-field}}. \tag{21}$$

E. Summary of the Method

In Fig. 5, the introduced SEEC method is sketched in a flow chart starting with the numerical stranding of a litz wire. In the numerical stranding, the positions of the individual strands are calculated for a unit cell. The coordinates of a unit cell are calculated only once, so reading from a memory is feasible in case of multiple calculations. An external magnetic field along an $\vec{\mathbf{e}}_1$ -directed winding is calculated, e.g., by an FEM simulation [18]. Due to periodically repeating twisting structures, this external magnetic field can always be mapped to a unit cell of the litz wire. Based on the positions of a unit cell and the external magnetic field contributions, the system of equations is set up and solved afterwards. The strand currents are calculated to determine the losses in the litz wire strands P_{curr} as well as the internal magnetic field. The losses $P_{\mathrm{H-field}}$ are caused by the magnetic field external to a certain strand, composed of internal and external magnetic field.

While the sweep of a frequency range requires only the repetitive solution of the equation system for each scanning point, the system of equations must also be set up repetitively if the litz wire properties are varied.

TABLE II
SPECIFICATIONS OF THE LITZ WIRES (*LW 1-14*) INVESTIGATED WITH THE PROPOSED MODELING APPROACH

litz wire	N	d_s (mm)	twisting structure	pitch lengths (mm)	config. cf. Fig.7	diameter litz wire (mm)	Length unit cell (mm)
lw 1	49	0.1	7 x 7	(30 x 15) mm (*calc.)*	-	1.0	30
lw 2	245	0.1	4 x 3 x 20.4	(37 x 37 x 29) mm (*real*) (36.7 x 36.7 x 27.6) mm	1	2.2	110
lw 3	245	0.1	4 x 3 x 20.4	(30 x 15 x 10) mm	1	2.2	30
lw 4	245	0.1	4 x 3 x 20.4	(36.7 x 36.7 x 27.6) mm	2	-	110
lw 5	245	0.1	4 x 3 x 20.4	(-37 x 37 x 29) mm (-36.7 x 36.7 x 27.6) mm	1	2.2	110
lw 6	245	0.1	7 x 35	(37 x 29) mm (36.7 x 27.6) mm	3	2.2	110
lw 7	1000	0.071	5 x 5 x 40	(46 x 26 x 15) mm (43.7 x 26.2 x 14.6) mm	4	3.3	131
lw 8	1000	0.071	5 x 5 x 40	(30 x 15 x 10) mm	4	3.3	30
lw 9	1000	0.071	5 x 5 x 40	(43.7 x 26.2 x 14.6) mm	5	3.3	131
lw 10	1000	0.071	5 x 5 x 40	(43.7 x 26.2 x 14.6) mm	6	-	131
lw 11	1000	0.071	7 x 4 x 35.7	(46 x 26 x 15) mm (43.7 x 26.2 x 14.6) mm	7	3.3	131
lw 12	1000	0.071	7 x 4 x 35.7	(43.7 x 26.2 x 14.6) mm	8	-	131
lw 13	1000	0.071	4 x 4 x 62.5	(43.7 x 26.2 x 14.6) mm	9	3.3	131
lw 14	245	0.1	4 x 3 x 20.4	(-38.6 x 25.7 x 15.4) mm	1	2.2	77

The number of strands *N*, the diameter of the strands d_s, the twisting structure, the diameter of the litz wire, the pitch length, as well as the length of a unit cell are listed. Some of the simulated litz wires are also available as prototypes, allowing to provide data on exact pitch lengths (real, black). From this data, pitch lengths for the simulated litz wires (calc., grey) are derived. The notation for the pitch lengths is based on that of the twisting structure, where the last number is the pitch length of the first twisting step. Note that a deviation of 5% from the real pitch lengths in the model is allowed to minimize the length of the unit cell. The structure in a cross-section of the litz wire is described by the configuration (config.) and can be found in Fig. 6.

III. MODELING AND VALIDATION OF SKIN EFFECT

According to [1]–[4], in many cases, skin and proximity losses can be calculated separately. Thus, the two effects are validated separately for the numerical model introduced in Section II. First, the skin effect in real litz wires is examined in detail in the model assuming a $\vec{\mathbf{e}}_1$-directed litz wire. In the numerical calculation, the litz wires are excited with a sinusoidal current of the amplitude $\underline{i} = 1$ A and all external magnetic fields $\hat{H}_{\mathrm{ex}}$ are zero. In order to include the entire litz wire structure, a unit cell is used. The detailed specifications of the litz wires investigated in this article are summarized in Table II and the structure of the litz wire is shown in Fig. 6 by means of a cross-section.

The strand currents are calculated for a litz wire with the fast numerical method. As shown in Fig. 7, the $(7 \times 7)_{49}$ litz wire (*lw 1*) has a sub-bundle located in the center which does not change its position radially along the axis of the litz wire. In analogy to the current displacement in round conductors with increasing frequency, the outer bundles carry higher current densities than the inner bundles (cf. Fig. 7). With higher rms values of the current densities in the outer bundles, the losses also increase according to (16). Imperfect twisting at top bundle level causes high strand currents [21], which is confirmed in Fig. 8. Within a $(4 \times 3 \times 20.4)_{245}$ litz wire (*lw 2*) [cf. Fig. 8(a)], sub-bundles do not remain in the center of the litz wire and strand current amplitudes are reduced compared to the $(7 \times 35)_{245}$ litz wire (*lw 6*) [cf. Fig. 8(c)]. For an ideal $(4 \times 3 \times 20.4)_{245}$ litz wire without inner bundles, current densities in all bundles would be expected to be equal.

Therefore, the question arises whether the different current densities calculated in the bundles of Fig. 8(a) are in line with reality. The calculation with the proposed method confirms the assumption that with the symmetrical configuration *lw 4* [cf. Fig. 8(b)], a similar current density occurs in all bundles. In this article, a symmetrical configuration is generated by packing the specific group of strands or sub-bundles into the smallest possible bundle with a round cross-section for each twisting step. In case of symmetrical packing, the radius of the modeled litz wire becomes larger than with a realistic litz wire. Using the numerical stranding procedure described in Section II, the strands can instead be placed within the cross-section with the realistic diameter of a litz wire without overlap. The difficult question whether the numerical modeling of the individual strand positions corresponds exactly to the case of a real litz wire is not answered in this article. It is concluded from Fig. 8(a) and (b) that the exact placement of strands in a litz wire actually has an effect on current densities in the bundles. In the following, the influence of the placement is not assumed to be crucial if symmetrical packing and numerical stranding (cf. Section II) give similar losses.

The frequency-dependent increase of skin losses is described by the skin factor, which is defined as follows:

$$D_{\mathrm{skin}} = \frac{P_{\mathrm{curr}}(f) + P_{\mathrm{H-field}}(f)}{|\underline{i}|^2 R_{\mathrm{dc}}} \quad \text{where} \quad \overline{\hat{H}^2}_{\mathrm{ex}} = 0\ \mathrm{A/m}\,. \tag{22}$$

For validation, the numerical calculation of D_{skin} is compared with measurements. All measurements related to the skin effect

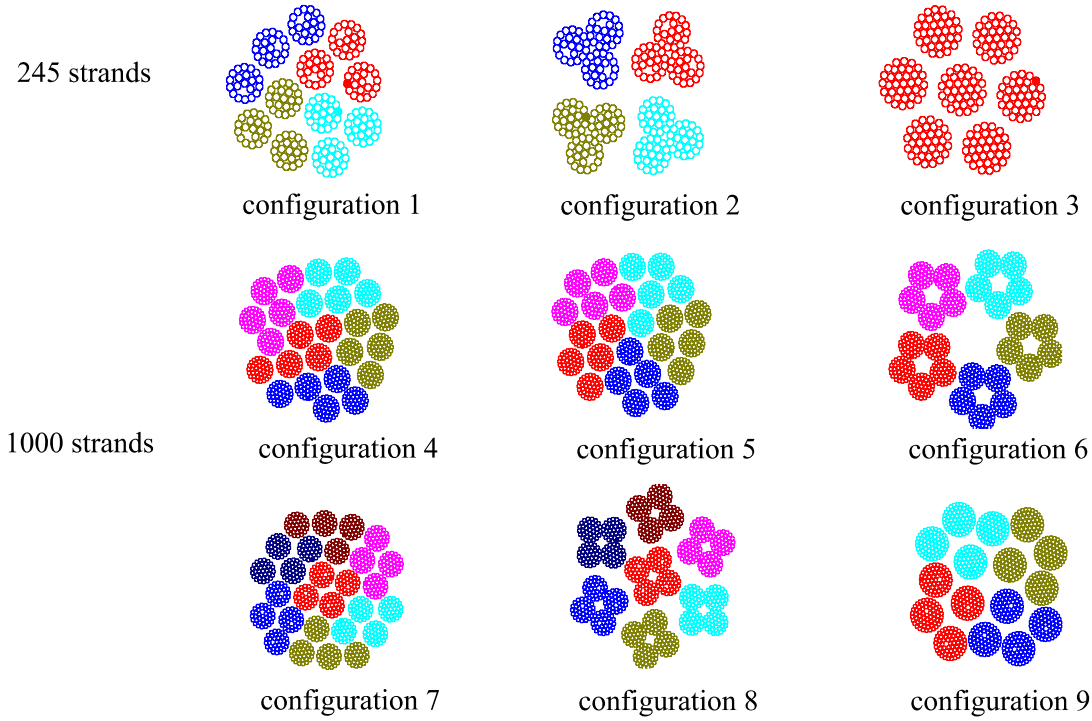

Fig. 6. Structure of different litz wires is shown by a cross-section of a modeled unit cell. Thereby, the twisted sub-bundles of bundle level 1 have the same color. Although the twisting structure (cf. Table II) is the same, different configurations are examined for a validation of the numerical method.

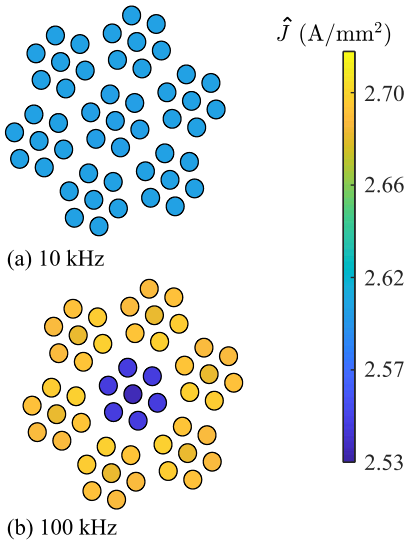

Fig. 7. Amplitude of the current density $\hat{J}$ in the strands of a type 7×7 litz wire (*lw 1*) with 49 strands, calculated using the fast numerical method at a frequency of (a) 10 kHz and (b) 100 kHz.

were done using the small signal impedance analyzer, Agilent 4294A. For the measurement, pieces (approx. 50 cm) of the litz wires with soldered ends were connected in a loop to the adapter (16047E Lead Component Test Fixture) of the impedance analyzer as shown in [1]. In keeping with [7], the measurements and calculations yield values for D_{skin}, which lie between a perfectly twisted litz wire (ideal litz wire) and a round wire. Deviations between measurements and numerical calculations are less than 20% up to frequencies of 10 MHz (cf. Fig. 9). These might be based on the error of Bessel function approach, on further named simplifications of the SEEC method or on the deviation of the modeled unit cell from a real litz wire. Due to the higher current densities in the single strands of the outer bundles (cf. Fig. 8), the ac resistance of the $(7 \times 35)_{245}$ litz wire is up to 50% higher compared to the $(4 \times 3 \times 20.4)_{245}$ litz wire. The measured and calculated skin factor of the $(4 \times 3 \times 20.4)_{245}$ litz wire is close to an ideal litz wire. Additionally, the results with PEEC method in Fig. 9 show a slight deviation to the calculations with SEEC method in the range from 50 kHz to 1 MHz. The reasons for a deviation and the simulation conditions are described in Table III.

The calculated skin losses of the unit cells of *lw 2–5* behave almost identically for the entire frequency range up to 10 MHz (cf. Fig. 10). However, the litz wires *lw 3–5* differ from *lw 2* by the pitch lengths or the pitch direction of the topmost twisting step. Their common feature is the same twisting structure $(4 \times 3 \times 20.4)_{245}$. Although the distribution of the strand currents differs from that of *lw 2* [cf. Fig. 8(a) and (b)], litz wire *lw 4* with a symmetrical structure has similar skin losses. It would appear that the different losses of the individual bundles in Fig. 8(a) are the same in total.

To verify these results, further structures of litz wires with 1000 strands (*lw 7–13*) are considered using the SEEC. In practice, a perfect radial permutation, which is characteristic of an ideal litz wire, is difficult to realize with more than six bundles [21]. In Fig. 11, it is shown that even litz wires (cf. *lw 7*) with five bundles in the top level may have significantly higher losses than the ideal litz wire. One explanatory approach is that the manufacturer has given priority to the packing factor over keeping symmetrical bundle positions. As a result, a bundle

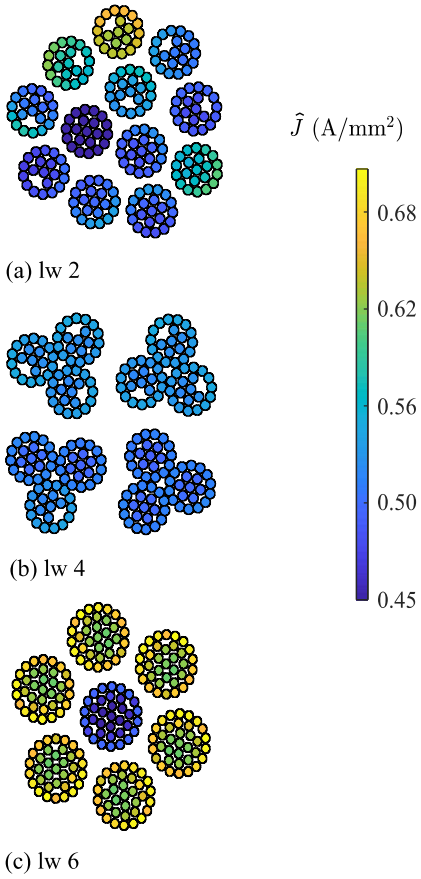

Fig. 8. Amplitude of the current density $\hat{J}$ in the strands of (a), and (b) type $(4 \times 3 \times 20.4)_{245} \times 0.1$ mm and (c) type $(7 \times 35)_{245} \times 0.1$ mm litz wire, calculated using the fast numerical method at 100 kHz. Note that the current density does not only depend on the cross-section shown but on the whole unit cell.

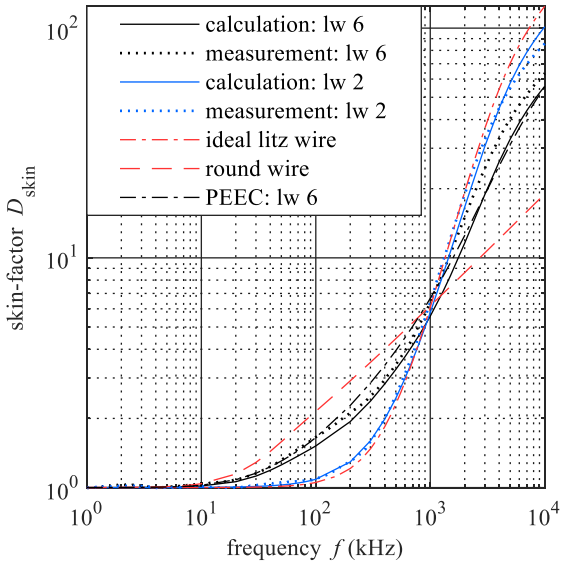

Fig. 9. Measurement and numerical calculation of the frequency-dependent skin factor D_{skin} for different twisting structures of a litz wire consisting of 245 strands with a diameter of 0.1 mm (cf. Table II). In addition, the analytic results for a perfectly twisted (ideal) litz wire and a round conductor with the same dc resistance are visualized. The results are compared with the PEEC method. Computation times for *lw 6* using SEEC and PEEC can be found in Table III.

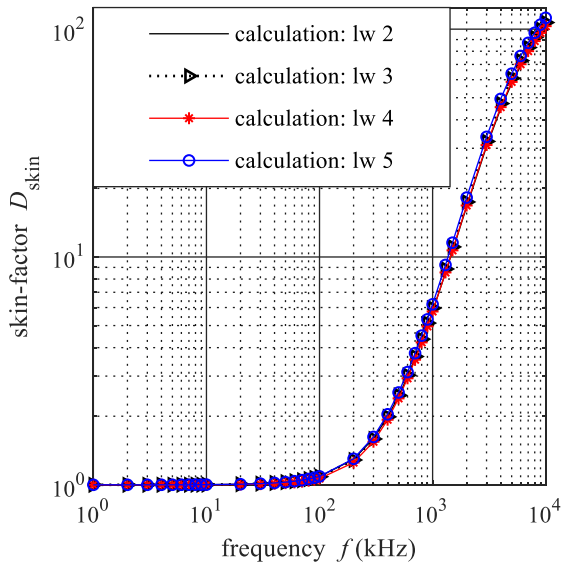

Fig. 10. Numerical calculation of the frequency-dependent skin factor D_{skin} for different structures (unit cells) of a litz wire consisting of 245 strands with a diameter of 0.1 mm (cf. Table II).

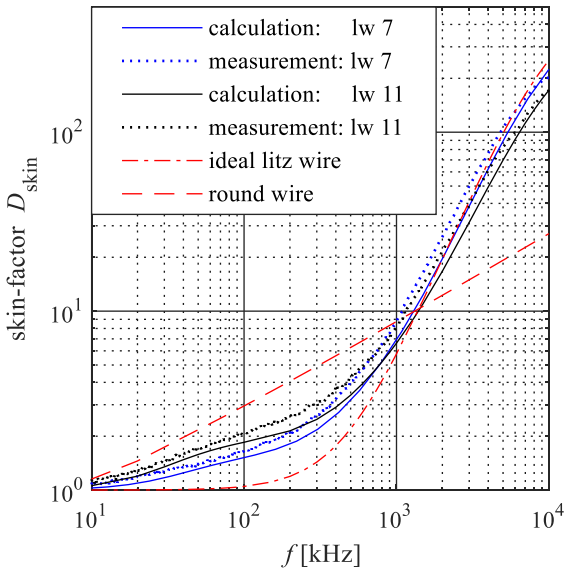

Fig. 11. Measurement and numerical calculation of the frequency-dependent skin factor for different twisting structures of a litz wire consisting of 1000 strands with a diameter of 0.071 mm (cf. Table II). The skin factor D_{skin} is plotted for frequencies up to 10 MHz.

slipped into the middle. If this effect is also considered in the model (see configuration 4), deviations between measurements and numerical calculations are less than 20%. Nevertheless, the stranding of the bundles is a manufacturing problem. If the manufacturer is able to better control the positions of the outer bundles in the top twisting step, this results in a structure without a central bundle and with a high packing density. The skin factor of such a $(5 \times 5 \times 40)_{1000}$ litz wire should be close to an ideal litz wire. This is confirmed by the numerical calculations with two unit cells of this litz wire (cf. Fig. 12), one with symmetrical (*lw 10*) and one with a more realistic arrangement of the top

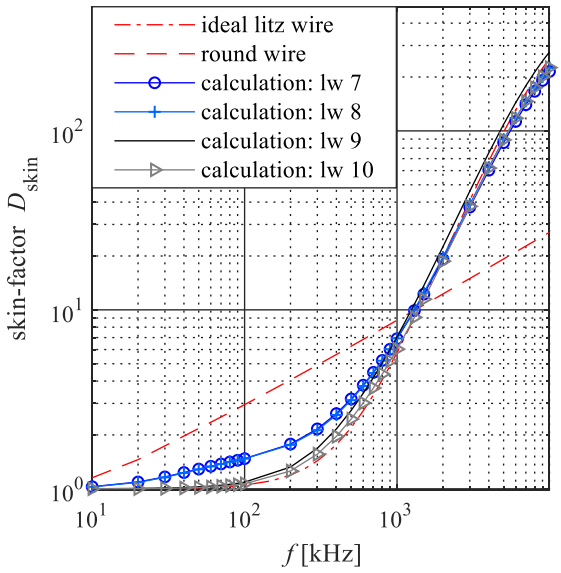

Fig. 12. Numerical calculation of the frequency-dependent skin factor for different configurations (cf. Fig. 6) of a litz wire consisting of 1000 strands (cf. Table II). The skin factor D_{skin} is plotted for frequencies up to 10 MHz. In addition, the analytic results for a perfectly twisted (ideal) litz wire and a round conductor with the same dc resistance are visualized.

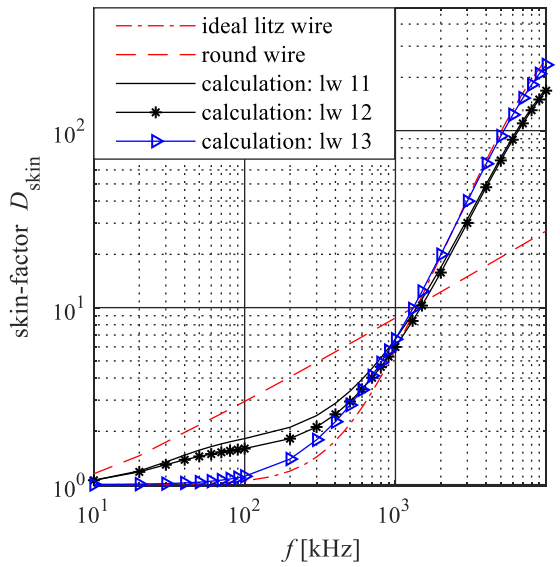

Fig. 13. Fast numerical calculation of the frequency-dependent skin factor for different twisting structures of a litz wire consisting of 1000 strands (cf. Table II). The skin factor D_{skin} is plotted for frequencies up to 10 MHz. In addition, the analytic results for a perfectly twisted (ideal) litz wire and a round conductor with the same dc resistance are visualized.

bundles (*lw 9*). Furthermore, the numerical calculations, e.g., *lw 7* and *8*, support the fact that the pitch lengths have a minor effect on skin losses (see Fig. 12). The comparison of the litz wires with central bundle (*lw 11 and 12*) verifies that the exact placement of the individual strands is of secondary relevance, even if a variation of up to 15 % is determined for skin losses (see Fig. 13). The twisting of groups of five bundles seems to be more difficult to control than groups of four, which would be preferable from this point of view. Furthermore, this $(4 \times 4 \times 62.5)_{1000}$ twisting structure shows a similar performance to a "well twisted" $(5 \times 5 \times 40)_{1000}$ structure in Fig. 13. Note that the number of strands of a bundle at strand level is technologically limited. If the number of strands as well as the strand diameter are given and the number of bundles in a single twisting step is limited, the remaining degree of freedom is to increase the number of twisting steps. However, the maximum number of bundle levels is subject to costs and manufacturability of a litz wire. Depending on the application, more than five bundles in a single bundle level may therefore be reasonable.

For the skin effect, we conclude the following. In order to obtain a perfect radial permutation of the bundles, probably no more than five bundles should be twisted in a step. The proposed method calculates these results on the basis of the current sharing between the individual strands depending on the complex twisting structure. Using different unit cells, it could be shown that pitch lengths and pitch directions have a minor effect on skin losses, which is also demonstrated in [21]. For the litz wires examined, skin losses differ by up to 15% due to a variation of strand positions. This is also a good confirmation with method [13], which requires orders of magnitude less computing time due to its analytical formulation and provides an accurate prediction of skin losses. In contrast to [13], however, the proposed technique also works well for more widely spaced strands, as the local magnetic field of strand currents external to a particular strand is considered. Furthermore, the method can be used for types of litz wire with a nonideal structure such as *lw 7* and with rectangular cross-sections. Measurements and calculations for litz wires with 1000 strands (cf. Fig. 11) match as well as for litz wires with 245 strands (cf. Fig. 9). Compared to previous numeric approaches [17], [18], the SEEC method based on strand elements requires computation time reduced by an order of magnitude. Losses of a litz wire with 1000 strands are calculated in about 2 min on a personal computer (cf. Table III).

The total calculation time includes the time to set up the unit cell/model and to solve the system of equations. The SEEC method is implemented in the programming language MATLAB. For the calculation and comparison with the PEEC method, a discretization level 3 was selected, which implies that each strand is resolved with 13 filaments. Using this level, a deviation of 10% from a reference loss simulation with discretization level 8 has been verified for a frequency 100 kHz and an average square magnetic field of 1000 A/m [23]. In contrast to the SEEC, the accuracy of the PEEC method is highly dependent on the discretization level of an individual strand. Note that for both methods, the same pitch lengths, the same lengths of the unit cells, and number of cross-sections in a unit cell are used (cf. Table II). A direct comparison of the accuracy of the two methods is not feasible because an exactly identical positioning of the strands cannot be ensured. Nevertheless, the example shows that PEEC method requires a much higher computation time than SEEC and calculation results of SEEC and PEEC are similar in Fig. 9.

IV. Modeling and Validation of Proximity Effect

Besides the skin effect, the proximity effect has a significant impact on losses in real litz wires. For the investigation of

TABLE III
CPU TIME ON A PERSONAL COMPUTER (CPU-TYPE: INTEL CORE I7-3632QM; NUMBER OF CORES: 4; RAM MEMORY: 7.8 GB) TO CALCULATE LOSSES FOR SEVERAL LITZ WIRES AS A FUNCTION OF FREQUENCY (40 FREQUENCY POINTS) USING THE PROPOSED NUMERICAL METHOD (SEEC) AND USING PEEC ACCORDING TO [17]

litz wire	number of strands	method	CPU time [sec]		
			unit cell/ model	solve	total
lw 6	245	SEEC	15	5	20
lw 6	245	PEEC	1700	14300	16000
lw 11	1000	SEEC	60	50	110

The total calculation time includes the time to set up the unit cell/model and to solve the system of equations. The SEEC method is implemented in the programming language MATLAB. For the calculation and comparison with the PEEC method, a discretization level 3 was selected, which implies that each strand is resolved with 13 filaments. Using this level, a deviation of 10% from a reference loss simulation with discretization level 8 has been verified for a frequency 100 kHz and an average square magnetic field of 1000 A/m [23]. In contrast to the SEEC, the accuracy of the PEEC method is highly dependent on the discretization level of an individual strand. Note that for both methods, the same pitch lengths, the same lengths of the unit cells, and number of cross-sections in a unit cell are used (cf. Table II). A direct comparison of the accuracy of the two methods is not feasible because an exactly identical positioning of the strands cannot be ensured. Nevertheless, the example shows that PEEC method requires a much higher computation time than SEEC and calculation results of SEEC and PEEC are similar in Fig. 9.

the proximity effect with the help of the numerical model, an $\vec{e}_1$ -directed litz wire with soldered ends is assumed. The litz wire is exposed to a homogeneous sinusoidal magnetic field $\overline{\hat{H}}_{\mathrm{ex}}$ perpendicular to $\vec{e}_1$ over its length l_{litz}. The total litz wire current $\underline{i}$ is zero. Nevertheless, the exciting magnetic field generates equalizing currents between single strands, producing losses (P_{curr}). The frequency-dependent increase of proximity losses is determined by the proximity factor D_{prox}, which is defined as follows (here, κ is the conductivity of copper):

$$D_{\mathrm{prox}} = \frac{P_{\mathrm{curr}}\left(f\right) + P_{\mathrm{H-field}}\left(f\right)}{\frac{1}{\kappa} l_{\mathrm{litz}} \overline{\hat{H}^2}_{\mathrm{ex}}} \text{ where } \underline{i} = 0 \text{ A} . \quad (23)$$

The numerical calculation of D_{prox} is validated in Figs. 14 and 15. All measurements related to the proximity effect were conducted using the measurement setup specified in [1], which consists of a magnetic circuit of U93/76/30 cores (material Ferroxcube 3F4) with air gaps. In this setup, the DUTs are exposed to a homogeneous magnetic field and the impedance of the excitation coil is measured. The numerical calculations of the proximity effect, which are also shown in [13], [17], [21], are compared to measurements using a custom-made setup. The tendencies of the numerical calculation are in good agreement with the measurement, cf. Figs. 14 and 15. Thereby, all results are generated as a function of the frequency and at a given length of the litz wire.

Calculations also show litz wire *lw 6*, which has a poor performance in case of skin loss due to the middle bundle, even performs better than *lw 2* with regard to the proximity effect. On the other hand, *lw 5* has the worst performance regarding proximity losses, but has low skin losses. These results

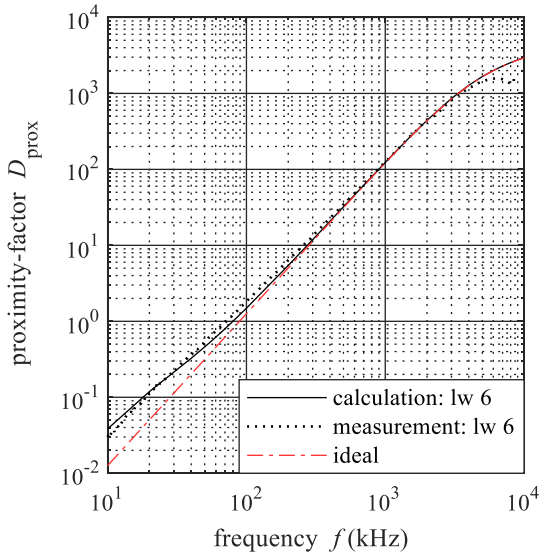

Fig. 14. Measurement and numerical calculation of the frequency-dependent proximity factor for type $(7 \times 35)_{245}$ litz wire *lw 6* (two bundle-levels) with a length $l_{\mathrm{litz}} = 0.155$ m (cf. Table II). In order to model the entire litz wire, the structure of the unit cell is periodically continued. The bundles on strand level and top level are twisted in the same direction. Therefore, pitch lengths are both positive.

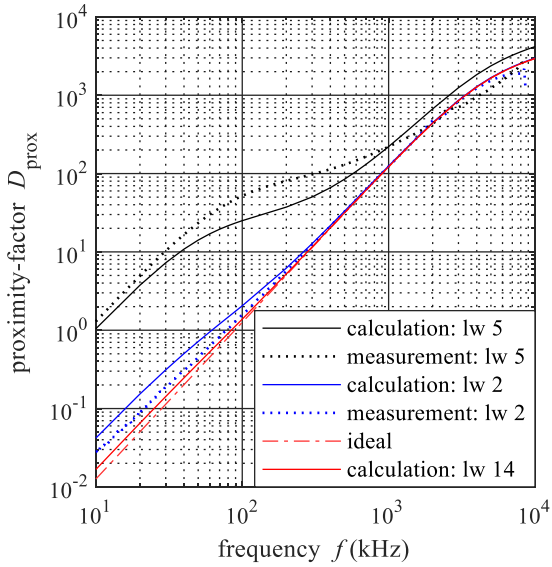

Fig. 15. Measurement and numerical calculation of the frequency-dependent proximity factor for various type $(4 \times 3 \times 20.4)_{245}$ litz wires with a length $l_{\mathrm{litz}} = 0.155$ m (cf. Table II). In order to model the entire litz wire, the structure of the unit cell is periodically continued. The bundles on strand level and middle bundle level are twisted in the same direction. In case of *lw 5, 14*, the bundles on top level are twisted in the opposite direction.

are explained by the absolute pitch length $l_{u,\mathrm{a}}$ of a bundle level u

$$\frac{1}{l_{u,\mathrm{a}}} = \sum_{k=u}^{u_{\max}} \frac{1}{l_u} \text{ where } u \in [1, u_{\max}] . \quad (24)$$

Thereby, l_u defines the pitch length of twisting step u and $u_{\max}$ the maximum number of twisting steps. The absolute twist rate of a sub-bundle $1/l_{u,\mathrm{a}}$ is the rotation relative to the global

coordinates of the litz wire. Due to the recursive twisting of sub-bundles, twist rates add up for positive pitch directions and subtract for negative pitch directions. Accordingly, the absolute pitch length $l_{2,\mathrm{a}}$ of sub-bundles in the coordinates of litz wire *lw 5* is infinite. As a result, the magnetic flux is not cancelled over the length of the sub-bundles and high losses due to equalizing currents will occur. Note that choosing the length of a unit cell equal to the smallest common multiple of all pitch lengths l_u, a sub-bundle with the rate $1/l_{u,\mathrm{a}}$ also receives an integer rotation in a unit cell. Because this applies to all twisting steps and the litz wire length l_{litz} corresponds approximately to the length of two unit cells, *lw 14* demonstrates almost ideal proximity losses. A change in the twisting direction does not necessarily have to cause excessive proximity losses, as long as the absolute pitch lengths of sub-bundles do not become too long, cf. Fig. 15. Generally, changing the pitch direction leads to an increase in absolute pitch lengths.

In accordance with the insights provided in [17], [21], it was found that the proximity factor D_{prox}, which refers to the sum of *N* individual strands, decreases with increasing length of the litz wire, and reaches the constant value above a certain length (cf. Fig. 16):

$$D_{\mathrm{prox}} = N D_{\mathrm{p}}. \tag{25}$$

According to (20), the proximity losses within strands are proportional to the total length of the litz wire l_{litz} and to the mean square of the magnetic field strength along the axis of the litz wire

$$P_{\mathrm{H-field}} \sim l_{\mathrm{litz}} \overline{\hat{H}^2}_{\mathrm{ex}}. \tag{26}$$

Further proximity losses P_{curr} are caused by induced equalizing currents between single strands, which are driven by the voltages $\underline{v}_n$ (see Fig. 4). When considering the proximity effect, these voltages strongly depend on the external magnetic field strength along the litz wire and it applies: $\underline{v}_n \approx \underline{v}_{n,\mathrm{ex}}$. Although the twisting of the bundles partly compensates the magnetic flux, a certain magnetic flux remains between the strands, which contributes to the induced voltage of a particular strand $\underline{v}_{n,\mathrm{ex}}$. These voltages are independent of l_{litz} when at least one unit cell is considered. They can vary significantly when a litz wire with a certain number of twist pitches is exposed to a low magnetic field in most of its length but to a strong field in a half pitch. The losses P_{curr} are determined as follows:

$$P_{\mathrm{curr}} = \frac{1}{R_n} \sum_{n=1}^{N} \left|\underline{v} - \underline{v}_n\right|^2 \sim \frac{1}{l_{\mathrm{litz}}} \sum_{n=1}^{N} \left|\underline{v}_{\mathrm{ex}} - \underline{v}_{n,\mathrm{ex}}\right|^2. \tag{27}$$

The loss ratio $P_{\mathrm{curr}}/P_{\mathrm{H-field}}$ decreases with the inverse square of litz wire length l_{litz}

$$P_{\mathrm{curr}}/P_{\mathrm{H-field}} \sim 1/l_{\mathrm{litz}}^2. \tag{28}$$

Conclusively, the proximity losses above a minimum litz length of the litz wire can be calculated independently of the bundle structure using the analytical formula (25) of a perfectly twisted litz wire. Furthermore, it is apparent from Fig. 15 that the losses due to equalizing currents have an effect primarily at low frequencies. This is already mentioned in [2], [6].

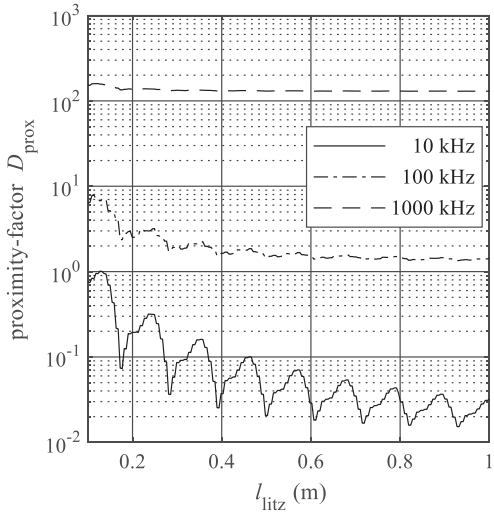

Fig. 16. Numerical calculation of the frequency-dependent proximity factor for a type $(5 \times 5 \times 40)_{1000}$ litz wire (cf. Table II). The bundles on various bundle levels are twisted in the same direction. Therefore, all pitch lengths are positive.

TABLE IV
CPU TIME ON A PERSONAL COMPUTER (CPU-TYPE: INTEL CORE I7-3632QM; NUMBER OF CORES: 4; RAM MEMORY: 7.8 GB) TO CALCULATE LOSSES FOR SEVERAL LITZ WIRES AS A FUNCTION OF FREQUENCY (40 FREQUENCY POINTS) TO CALCULATE THE MINIMUM LENGTH AT WHICH EQUALIZING CURRENTS HAVE A NEGLIGIBLE EFFECT ON PROXIMITY LOSSES

litz wire	number of strands	number of scanning points	CPU time: solve
lw 2	245	10	10 x 4 sec
lw 7	1000	10	10 x 30 sec

We consider already 10 scanning points to be sufficient to estimate this minimum length of a litz wire.

Equalizing currents cannot be ignored in applications with short windings compared to the absolute pitch lengths $l_{u,\mathrm{a}}$ of a litz wire. For the selection of a suitable litz wire, the proposed numerical calculation method can be used to determine the minimum litz wire length at which equalizing currents have a negligible effect on losses. Unlike sampling in the frequency range (cf. Fig. 13), the matrices of the equation system (12) must be calculated repetitively for each litz wire length as in Fig. 16. This requires the CPU times to solve a single frequency point multiplied by the number of scanning points of the litz wire length, cf. Table IV.

Nevertheless, it is recommended to perform scans and variations over a wide range of values using analytical methods such as [13], because of the lower computational effort. The SEEC method is suitable to calculate realistic litz wire structures. A noncircular shape of the bundles and equalizing currents in the individual strands due to bundle effects are no limitation. Proximity losses depend strongly on pitch lengths and bundle

positions. Although the calculations in this article only use one special configuration of the complex bundle structure, calculation errors caused by variations of the strand positions compared to a real litz wire almost cancel out over the length of a unit cell. Thus, experiment and calculation match quite well.

V. Conclusion

The SEEC method presented in this article allows the investigation of losses for litz wires with a complex twisting structure. In the examples that have been presented, skin and proximity losses are calculated on a personal computer. With regard to the skin effect, it is found that the radial permutation of the bundles over the cross-section along the axis of a litz wire has a strong impact on skin losses. By contrast, the exact pitch lengths and directions of particular twisting steps are less relevant. It has been shown that imperfect radial permutation of five bundles in the top bundle level may result in significantly increased losses if the bundle positions are not precisely controlled during the manufacturing process. In order to avoid excessive losses with regard to the proximity effect, the absolute pitch lengths in the individual bundle levels must be short compared to the total length of the winding. Changing twisting direction at some bundle level generally increases the absolute pitch lengths. The proposed method is accurate for typical litz wires with a round and rectangular cross-section. The local magnetic field is calculated from the strand currents. It may therefore be considered that the method is accurate even for strong bundle level effects, for noncircular shapes of the bundles, as well as more widely spaced strands in a bundle. Numerical calculations using the SEEC and measurements of skin and proximity losses show quite good agreement up to a frequency of 10 MHz. Especially with regard to lower frequencies, short windings compared to the absolute pitch lengths and the manufacturing costs, the numerical method is feasible to select a suitable litz wire for a specific application or to design a litz wire considering realistic twisting structures. In certain cases, however, the losses of a real litz wire can be calculated more quickly. Above a minimum winding length, where equalizing currents are negligible, proximity losses may be calculated independently of the bundle structure with an analytical formula [1], [4], [7]. Scans and variations over a wide range of values predicting the worst case for, e.g., manufacturing variations should still be performed with analytical methods such as [13] if the computational effort is a strong restriction.

To further improve the calculation accuracy of the SEEC method, algorithms for the design of twisting structures need to be enhanced to produce a realistic packing density even for a bundle of strands. As an outlook, it would be valuable to model constructions with cylindrical bundles and various degrees of deviation from these. Such modeling would allow even more general conclusions with regard to individual twisting parameters.

Acknowledgment

The authors would like to thank Dr. Andreas Roßkopf for his valuable scientific input and discussions.

References

[1] H. Rossmanith, M. Doebroenti, M. Albach, and D. Exner, "Measurement and characterization of high frequency losses in nonideal litz wires," *IEEE Trans. Power Electron.*, vol. 26, no. 11, pp. 3386–3394, Nov. 2011.

[2] C. R. Sullivan, "Optimal choice for number of strands in a litz-wire transformer winding," *IEEE Trans. Power Electron.*, vol. 14, no. 2, pp. 283–291, Mar. 1999.

[3] J. Mühlethaler, "Modeling and multi-objective optimization of inductive power components," Dissertation, Dept. Elect. Eng., Eidgenössische Technische Hochschule Zürich, Zürich, Switzerland, 2012.

[4] J. A. Ferreira, "Analytical computation of AC resistance of round and rectangular litz wire windings," *IEE Proc. B Elect. Power Appl.*, vol. 139, no. 1, pp. 21–25, Jan. 1992.

[5] J. A. Ferreira, *Electromagnetic Modelling of Power Electronic Converters*. Berlin, Germany: Springer Science & Business Media, 1989.

[6] C. R. Sullivan and R. Y. Zhang, "Simplified design method for litz wire," in *Proc. 29th IEEE Annu. Appl. Power Electron. Conf. Expo.*, 2014, pp. 2667–2674.

[7] M. Albach, *Induktivitäten in Der Leistungselektronik: Spulen, Trafos Und ihre Parasitären Eigenschaften*. Wiesbaden, Germany: Springer Vieweg, 2017.

[8] X. Nan and C. R. Sullivan, "An equivalent complex permeability model for litz-wire windings," *IEEE Trans. Ind. Appl.*, vol. 45, no. 2, pp. 854–860, Mar./Apr. 2009.

[9] H. Rossmanith, M. Albach, J. Patz, and A. Stadler, "Improved characterization of the magnetic properties of hexagonally packed wires," in *Proc. 14th Eur. Conf. Power Electron. Appl.*, Aug./Sep. 2011, pp. 1–9.

[10] A. Stadler and C. Gulden, "Copper losses of litz-wire windings due to an air gap," in *Proc. 15th Eur. Conf. Power Electron. Appl.*, 2013, pp. 1–7.

[11] D. C. Meeker, "An improved continuum skin and proximity effect model for hexagonally packed wires," *J. Comput. Appl. Math.*, vol. 236, no. 18, pp. 4635–4644, 2012.

[12] T. Delaforge and H. Chazal, "Formal solution based on the magnetic potential for round conductive area," *IEEE Trans. Magn.*, vol. 54, no. 12, pp. 1–8, Dec. 2018.

[13] C. R. Sullivan and R. Y. Zhang, "Analytical model for effects of twisting on litz-wire losses," in *Proc. IEEE 15th Workshop Control Model. Power Electron.*, 2014, pp. 1–10.

[14] K. Umetani, J. Acero, H. Sarnago, O. Lucia, and E. Hiraki, "Simple fully analytical copper loss model of litz wire made of strands twisted in multiple levels," in *Proc. IEEE Appl. Power Electron. Conf. Expo.*, 2019, pp. 1257–1264.

[15] A. E. Ruehli and P. A. Brennan, "Efficient capacitance calculations for three-dimensional multiconductor systems," *IEEE Trans. Microw. Theory Techn.*, vol. 21, no. 2, pp. 76–82, Feb. 1973.

[16] A. E. Ruehli, "Equivalent circuit models for three-dimensional multiconductor systems," *IEEE Trans. Microw. Theory Techn.*, vol. 22, no. 3, pp. 216–221, Mar. 1974.

[17] R. Y. Zhang, J. K. White, J. G. Kassakian, and C. R. Sullivan, "Realistic litz wire characterization using fast numerical simulations," in *Proc. 29th Annu. IEEE Appl. Power Electron. Conf. Expo.*, 2014, pp. 738–745.

[18] A. Rosskopf, E. Bär, C. Joffe, and C. Bonse, "Calculation of power losses in litz wire systems by coupling FEM and PEEC method," *IEEE Trans. Power Electron.*, vol. 31, no. 9, pp. 6442–6449, Sep. 2016.

[19] G. Cerri, V. M. Primiani, and S. A. Kovyryalov, "Modelling of a litz-wire planar winding geometry for an accurate reactance evaluation," *IET Sci., Meas. Technol.*, vol. 4, no. 4, pp. 214–219, 2010.

[20] L. Giussani, M. Bechis, C. de Falco, and L. Di Rienzo, "An integral formulation for an array of wires in a 3-D magneto-quasi-static field," *IEEE Trans. Magn.*, vol. 54, no. 7, pp. 1–8, Jul. 2018.

[21] T. Guillod, J. Huber, F. Krismer, and J. W. Kolar, "Litz wire losses: Effects of twisting imperfections," in *Proc. IEEE 18th Workshop Control Model. Power Electron.*, 2017, pp. 1–8.

[22] B. A. Reese, R. Joseph, and C. R. Sullivan, "Improved litz-wire designs for the MHz range," in *Proc. IEEE 18th Workshop Control Model. Power Electron.*, 2017, pp. 1–8.

[23] A. Rosskopf, "Calculation of frequency dependent power losses in inductive systems with litz wire conductors by a coupled numeric approach," Dissertation, Dept. Inf. Technol. Elect. Eng., Friedrich-Alexander-Universität, Erlangen, Germany, 2018.

Stefan Ehrlich received the B.Sc. and the M.Sc. degrees in electrical engineering from the Friedrich-Alexander-University Erlangen-Nuremberg, Erlangen, Germany, in 2012 and 2015, respectively. He is currently working toward the Ph.D. degree in electrical engineering with the Fraunhofer Institute for Integrated Systems and Device Technology IISB, Erlangen, Germany.

His research interests include electromagnetic field theory, characterization, and modeling of inductive components.

Hans Rossmanith received the Dr.-Ing. degree from Erlangen University, Erlangen, Germany, in 1990.

From 1993, he was a Scientific Assistant with the Department of Electrical Engineering, Electronics and Information Technology, Friedrich-Alexander-University, Erlangen-Nuremberg, Bavaria, Germany. In 1999, he joined the Chair for Electromagnetic Fields. His research interests include electromagnetic field theory, electromagnetic compatibility, and numerical field calculation.

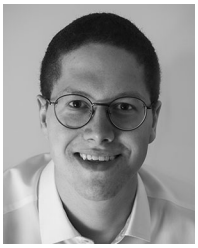

Marco Sauer received the B.Sc. degree in electrical engineering from the University of Erlangen-Nuremberg, Erlangen, Germany, in 2019.

He conducted his bachelor's thesis on the design of transformers for LLC resonant converters with the Chair of Power Electronics, University of Erlangen-Nuremberg, and in cooperation with the Fraunhofer Institute of Integrated Systems and Device Technology, Erlangen.

Christopher Joffe received the diploma degree in mechatronics from the Dresden University of Technology, Dresden, Germany, in 2011, and the Ph.D. degree from the Friedrich-Alexander-University Erlangen-Nuremberg, Erlangen, Germany, in 2019.

He is currently working with the Department of Vehicle Electronics, Fraunhofer Institute for Integrated Systems and Device Technology, Erlangen, Germany, where he is a Team Leader of the group RF Power Electronics and EMC. His research interests include inductive power transfer systems, resonant converters, application of new semiconductor devices, and EMC simulation.

Martin März received the Diploma degree in electrical engineering in 1988, and the Ph.D. degree in microwave excitation of CO_2 lasers from the Institute of Microwaves and Photonics at the University of Erlangen-Nuremberg, Erlangen, Germany, in 1995.

He started his career in the semiconductor division with Siemens (later Infineon AG), Munich, Germany. Since 2000, he has been the Head with the Power Electronics System Department, Fraunhofer Institute of Integrated Systems and Device Technology IISB, Erlangen, where he has been the Deputy Director since 2012, the Acting Director since 2018. In 2016, he was appointed as a Full Professor to the newly established Chair of Power Electronics. His research interests include innovative technologies for power electronics with a focus on very high power density and efficiency, thermal management, and cognitive power electronics.